Orbital and suborbital variations of productivity and sea surface conditions in the Gulf of Alaska during the past 54,000 years: Impact of iron fertilization by icebergs and meltwater

Oscar E. Romero[1,2], Leah J. LeVay[3], Erin L. McClymont[4], Juliane Müller[1,2], and Ellen A. Cowan[5]

[1]MARUM – Center for Marine Environmental Sciences, University of Bremen, Leobener Str. 8, 28359 Bremen, Germany. Orcid: 0000-0003-0209-3258

[2]Alfred Wegener Institute, Helmholtz Centre for Polar and Marine Research, Am Alten Hafen 26, 27568 Bremerhaven, Germany

[3]International Ocean Discovery Program, Texas A&M University, 1000 Discovery Dr, College Station, Texas 77845, USA. Orcid: 0000-0003-3031-7079

[4]Department of Geography, Durham University, Lower Mountjoy, Durham DH1 3LE, U.K. Orcid: 0000-0003-1562-8768

[5]Department of Geological and Environmental Sciences, Appalachian State University, Box 32067 Boone, NC 28608, USA. Orcid: 0000-0001-6512-5769

Corresponding author: Oscar E. Romero (oromero@marum.de)

Key points

Iron fertilization of marine waters linked to Cordilleran Ice Sheet iceberg discharge as driver of phytoplankton growth during the past 54 ka.

Occurrence of calcareous and siliceous primary producers was largely unaffected by low SST conditions during MIS 3 and MIS 2.

Tidewater glaciers impact on marine productivity dynamics of high-latitude coastal regions is essential to understand land-ocean interactions.

Abstract

As a high-nutrient and low-chlorophyll region, the modern Gulf of Alaska (GoA) is strongly impacted by the limitation of iron. Paleostudies along the Alaskan slope have mainly focused on reconstructing environmental conditions over the past 18 ka. Based on micropaleontological, biogeochemical and sedimentological parameters, we explore a sediment record covering the past 54 ka at Integrated Ocean Drilling Program Site U1419 to understand the impact of orbital and suborbital-scale climate variability on productivity and sea-surface conditions. Close to the Cordilleran Ice Sheet (CIS), Site U1419 is ideally located to elucidate how the evolution of a large ice mass and glacial processes affected orbital- and suborbital-scale changes in nutrients-(*e.g.*, iron) supply. Meltwater discharge from the northern CIS impacted sea surface dynamics of GoA coastal waters. The corresponding increase in bulk biogenic concentrations during Marine Isotope Stage (MIS) 3 and MIS 2 (54 – 17.3 ka) suggests a direct impact from iron fertilization. Cooling of surface waters played no primary role in the occurrence of primary producers. The inundation of the subaerially exposed continental shelf during the last deglacial (17.3-10 ka) warming could have served as a major micronutrients source. Low productivity after the last deglaciation suggests reduced iron availability. Our multiproxy approach reveals a more complete picture of late Quaternary productivity variations compared to earlier studies along the Alaskan margin. The impact of tidewater glaciers and meltwater discharge on past marine productivity and nutrient budget dynamics of high-latitude coastal regions is discussed.

1. Introduction

Located in the subarctic eastern Pacific, the Gulf of Alaska (GoA) is a high-nutrient, low-chlorophyll (HNLC) area where phytoplankton biomass is consistently low (Childers et al., 2005). Especially beyond the continental shelf break, coastal surface waters of the GoA are largely iron-limited (Boyd et al., 2007). As low bioavailability of the micronutrient iron critically limits primary producers' occurrence (Martin, 1990), increases in the iron supply mostly led to enhanced productivity in surface waters and carbon export to the seafloor of the GoA (Childers et al., 2005; Coyle et al., 2019; Strom et al., 2006, 2016). Iron fertilization is widely acknowledged to enhance primary productivity in high northern (Strom et al., 2006; 2016) and southern (Blain et al., 2007; Duprat et al., 2016) latitudes. Glaciers play a globally significant role as a source of iron to the marine surface waters (Hopwood et al., 2015). While marine sediment records show higher paleoproduction during glacials that are correlated with enhanced iron inputs in high southern latitudes (*e.g.*, Martínez-García et al., 2011), paleoceanographic records supporting links between productivity and glacier dust and/or iceberg discharge-mediated iron fertilization in the north-eastern Pacific Ocean are still scarce (Müller et al., 2018).

Paleoclimate reconstructions based on sediments deposited beneath waters close to the Alaskan margin has mainly focused on the physical and biological changes throughout the last deglaciation and the Holocene (Addison et al., 2012; Barron et al., 2009; Davies et al., 2011; Praetorius et al., 2018). However, it is still unclear how marine productivity and sea-surface conditions of GoA coastal waters responded to pulses of meltwater and iceberg discharge during Marine Isotope Stages (MIS) 2 and 3, when the Cordilleran Ice Sheet (CIS) was larger than present (Seguinot et al. 2016). Since primary producers occur in surface waters of the GoA north of 57°N are largely influenced by iron limitation (Boyd et al., 2007; Martin, 1990; Strom et al., 2006, 2016), understanding the delivery and impact of micronutrients in past geological times can be helpful in interpreting future trends of phytoplankton growth in response to global change. A remarkable recent discovery is that the occurrence of millennial-scale episodes of reorganized Pacific Ocean ventilation at Site U1419 reoccurs in phase with large deliveries of CIS ice-rafted debris (IRD) during the past 42 ka, indicating a close linkage between ice and ocean dynamics (Walczak et al., 2020). These events of increased IRD accumulation, termed Siku Events (SE), precede North Atlantic Heinrich Events (HE) by ~1300 years (Walczak et al., 2020). Since meltwater delivers iron to

the GoA (Childers et al., 2005; Crusius et al., 2011, 2017), the episodic iceberg discharges along the northern Alaskan margin might have also impacted the past nutrient availability of
99 surface waters overlying Site U1419.

Relative to many other areas of the subarctic Pacific Ocean, the northern GoA remains under-studied (Crusius et al., 2017). This limits our understanding of the important
102 processes controlling (paleo)productivity variations in the high-latitude Pacific such as the impact of iceberg discharge and the potential importance of bioavailable Fe delivery to this HNLC area. This study presents a high-resolution paleorecord of primary producers and sea-
105 surface temperatures (SST) for the past 54 ka at Integrated Ocean Drilling Program (IODP) Site U1419 (ca. 59°N, 145°W, Figure 1). We combine independent biogenic parameters indicative of variations of (*i*) ocean productivity (coccolithophorids, diatoms, bulk biogenic
108 components), (*ii*) sea ice cover ($IP_{25,}$ $C_{37:4}$, diatoms), and (*iii*) alkenone-based ($U^{K'}_{37}$-) SST, and compare these to the Site U1419 IRD record (Walczak et al., 2020). Our findings describe glacial-interglacial and millennial-scale changes in productivity as well as potential sources of
111 nutrient inputs, offering new evidence which help interpret the drivers of environmental change in the GoA during the last 54 ka.

114 **2. Study area**

2.1. Atmospheric and hydrographic settings, and ice dynamics

Surface waters overlying Site U1419 are iron-poor, nitrate-rich, and have low chlorophyll
117 concentrations. Two nutrient regimes are known in the GoA: an HNLC region in the centre of the Alaska Gyre, offshore of the Alaskan coast; and a low nutrient, high chlorophyll regime which is associated with the Alaska Coastal Current (ACC) (Childers et al., 2005). These
120 regimes are characterized by specific oceanographic conditions. Advection of deep eutrophic waters to the surface ocean coupled with micronutrient availability (*i.e*. iron) from land is typical of the HNLC region, while the low-nutrient, high chlorophyll region relies on the
123 advection of deep, nutrient-rich waters to supply macronutrients (*i.e*. nitrate) (Childers et al., 2005; Stabeno et al., 2004).

An annual cycle of nutrient drawdown and replenishment occurs in the euphotic zone of
126 waters overlying Site U1419, in response to the local ocean circulation. Wind-induced downwelling and easterly coastal winds cause a well-mixed water column in winter (Childers et al., 2005). Phytoplankton blooms are associated with the onset of annual stratification in

129 spring/summer, when increased light availability favors high productivity (Henson, 2007). A fall peak in chlorophyll concentrations is observed with the initial weakening of stratification (Henson, 2007). Although freshwater input associated with glacier meltwaters causes
132 stratification of the upper water column (Stabeno et al., 2004), it also fertilizes the ocean surface (Crusius et al., 2017). Presently, mostly land-derived rainfall water is transported along the southwest Alaskan coast through the ACC (Kipphut, 1990).

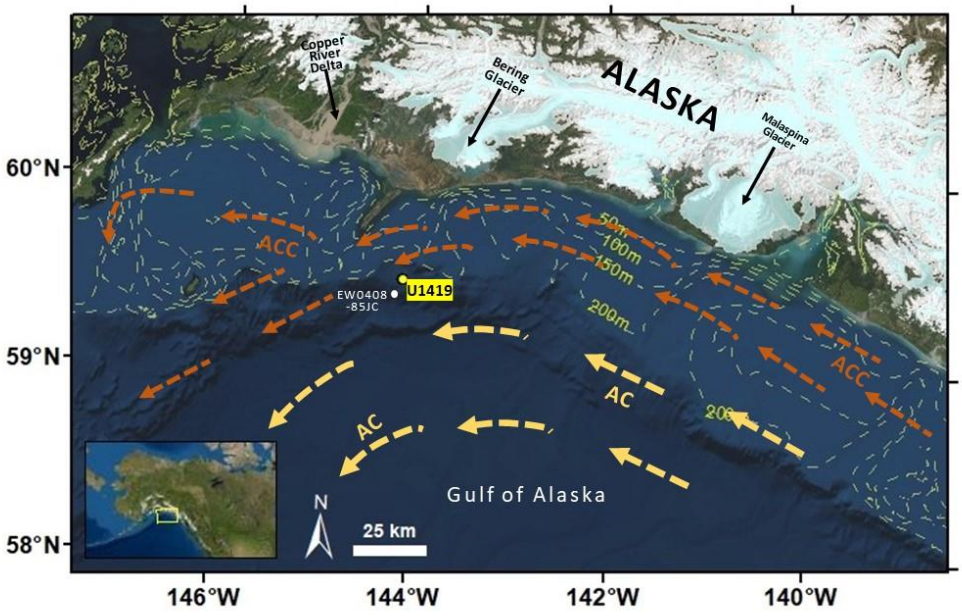

135

Figure 1. Map showing the study area in the high latitude north-eastern Pacific Ocean. Location of IODP Site U1419 (yellow dot, 59° 31.9'N, 144° 8.0'W; 698 m depth;
138 Expedition 341, Jaeger et al., 2014a) and EW0408-85JC (white dot; Addison et al., 2012; Barron et al., 2009; Davies et al., 2011; Praetorius et al., 2018). AC: Alaska Current; ACC: Alaska Coastal Current.

141 The circulation in the GoA is dominated by a two-current system: the subarctic gyre in the ocean basin, including the Alaska Current (AC), and the ACC on the continental shelf (Figure 1; Stabeno et al., 2004). The ACC flows northwards along the Alaskan continental shelf,
144 forced by alongshore winds, and it is fueled with large freshwater runoff by glacier and river discharge (Stabeno et al., 2004; Crusius et al., 2017). The AC is sourced from warm mid-latitude currents of the North Pacific flowing eastwards, termed the North Pacific Current
147 (Stabeno et al., 2004). The AC turns south-westward at the northern border of the GoA and forms the beginning of the Alaskan Stream (Freeland, 2006; Stabeno et al., 2004). The flow of water masses in the study area is further complicated by small, transient eddies
150 frequenting the GoA shelf, which combine with large, long-lasting eddies that travel along

the continental slope for 2–3 years (Crawford et al., 2007). These eddies may also influence transport and mixing of nutrients to the euphotic zone of the GoA.

Iron sources to the euphotic zone in the GoA are: atmospheric dust, glacier flour (fine ground dust containing Fe) derived from meltwater and iceberg rafting (Müller et al., 2018), shallow shelf sediments (Crusius et al., 2011), hydrothermal inputs (Boyd & Ellwood, 2010) and eddies (Crusius et al., 2017). An immediate response of phytoplankton to iron fertilization (Boyd et al., 2007) is indicated by a twofold increase in the particulate organic matter C:N ratio when iron is available (Martin, 1990). In coastal GoA waters, delivery of bioavailable iron has four main sources: (*i*) glacier flour transported by rivers (Crusius et al., 2011), (*ii*) dust from exposed glacial sediments and river mouths during the fall (such as the Copper River, Crusius et al., 2011), (*iii*) sea level rise and associated flooding (Davies et al., 2011), and (*iv*) sediments stored on the shelf and slope (Praetorious et al., 2015). Glacial meltwater dominates delivery of dissolved iron to the coastal GoA (Schroth et al., 2009). For the purpose of this paper and according to Crusius et al. (2017), the terms “meltwater,” “glacial meltwater,” and “freshwater” are considered synonymous and primarily reflect discharge from rivers which has originated from glacier melt.

Freshwater discharge into the coastal GoA strongly varies on seasonal and interannual timescales (Wang et al., 2004). From November to April, winter precipitation is mainly stored as snow, and freshwater discharge is reduced to a minimum. Freshwater discharge rises sharply from May due to (*i*) increasing precipitation and (*ii*) above-freezing temperatures. Summer discharge remains high until September because of melting snow and some glacier melt. River discharge decreases rapidly in October, and reaches a basic flow in December as temperatures drop below 0°C (Wang et al., 2004).

3. Materials and Methods

3.1. Site U1419

In May-July 2013, IODP Expedition 341 drilled a transect of sites (U1417-U1421) in the GoA, across the Surveyor Fan to the continental shelf offshore of the St. Elias Mountains. The main objective of Expedition 341 was to investigate a glacially-eroded sedimentary record during a cooling climate (Miocene through to Pleistocene) with increasing intensity of glaciations (Jaeger et al., 2014a). Site U1419 is located at 59°31.93’N-144°8.03’W and was drilled to 193.72m CCSF-B (meters core composite depth below sea floor, method B; Jaeger

et al., 2014b) at 698 m water depth on the northern Alaskan continental slope. Here we focus on the uppermost 47 m (2-54 ka) of the cored sequence, where high recovery (>87%, Jaeger et al., 2014a) allows development of a high-resolution reconstruction of primary production and sea-surface conditions constrained by foraminiferal radiocarbon dates (Walczak et al., 2020).

3.2. Age model and sedimentation rates

The detailed chronology for Site U1419 between the present and ~54 ka is based on 82 ^{14}C dates on pairs of benthic-planktic foraminifera spanning the past ~50 ka and 28 paired measurements from <18 ka in the co-located core EW0408-85JC, as published in detail by Walczak et al. (2020). Radiocarbon measurements on benthic and planktonic foraminifera were calibrated using the IntCal13 curve (Reimer et al., 2013). A constant benthic reservoir correction (R) of 1200 +/- 600 a was used, whereas a variable planktonic reservoir correction (R) (average 370 a +/- 350 a) reflected modelled circulation changes and the measured benthic - planktonic differences in the core. The age model has an average 1δ-uncertainty of 210 cal. yr. The Mass Accumulation Rates (MARs) calculated in this study (Suppl. Material) use the 50th percentile values of Walczak et al. (2020). All data presented here refer to the calibrated ages.

3.3. Bulk sediment components

Biogenic silica (bSi, opal) was measured using a sequential leaching technique in the MARUM Opallab (University of Bremen, Bremen, Germany) (Müller & Schneider, 1993). The precision of the sequential leaching technique is better than 0.5% (Müller & Schneider, 1993). The resolution of bSi measurements (at least every 40 cm) is lower than the diatom counts (every 10 to 40 cm). This is because the diatom values are at/close to zero in many Site U1419 samples, this making the bSi content almost undetectable (Müller & Schneider, 1993).

The total organic carbon content (wt. % TOC) was determined by means of a Vario MAX C elemental analyzer after decalcification with 1.3 N hydrochloric acid. Inorganic carbon (% carbonate) was measured using coulometry at the Department of Geological Sciences, University of Florida (Gainesville, Florida, U.S.) and at the International Ocean Discovery Program, Texas A&M University (College Station, Texas, U.S.). In total, 284 samples were dried in an oven at 50°C, ground with a mortar and pestle, weighed on a microbalance, and digested using 2 N HCl. The coulometer measures the micrograms C released from the

digestion of the sample. Carbonate is then calculated as $CaCO_3$ = µg C * 8.333 / sample mass (µg). Replicate measurements indicate an error of up to 0.19% carbonate.

3.4. Alkenone and IP_{25} analysis and SST Estimations

Alkenones were extracted from 1-2 g freeze-dried and homogenized sediments which had been sampled every 50 cm on average (but as low as every 2 cm), following Kim et al. (2002). Alkenones were analyzed by capillary gas chromatography: a gas chromatograph (HP 5890A) was equipped with a 60 m column (J&W DB1, 0.32 mm x 0.25 µm), a split injector (1:10 split modus), and a flame ionization detector (GC-FID). Quantification of the individual C_{37} alkenone concentrations ($C_{37:2}$, $C_{37:2}$ and $C_{37:4}$) was achieved using nonadecanone as an internal standard. Given recent suggestions of a potential sea ice contribution to $C_{37:4}$ (Wang et al., 2020) we present concentrations of $C_{37:3}$+$C_{37:2}$ separate from $C_{37:4}$, although the overall patterns remain the same. The relative abundance of $C_{37:4}$ is expressed as a percentage of the total C37 alkenones (%$C_{37:4}$)(Rosell-Melé et al., 2002).

To determine SSTs using the alkenone unsaturation index $U^{K'}_{37}$, alkenones were analyzed by gas chromatography with chemical ionization mass spectrometry (GC-CIMS), following the instrument method described in detail by Sanchez-Montes et al. (2020). The U^{K}_{37}' index is calculated from the relative abundances of the di- and tri-unsaturated C_{37} methyl alkenones as defined by Prahl & Wakeham (1987):

$$U^{K'}_{37} = (C_{37:2})/(C_{37:2} + C_{37:3})$$

The $U^{K'}_{37}$ values were converted into SSTs by applying the core-top compilation of Müller et al. (1998; U^{K}_{37}' = 0.033*T + 0.044), which aligns closely with a culture calibration (Prahl et al., 1988; $U^{K'}_{37}$ = 0.034*T + 0.039). Although alternative high-latitude SST calibrations are also available (Suppl. information) the same trends are recorded regardless of calibration. Using multiple extractions and analyses of a sediment sample used as a laboratory internal reference from the South Atlantic, the precision of the measurements ($\pm 1\sigma$) was calculated to be better than 0.003 $U^{K'}_{37}$ units (or 0.1°C) (Sanchez et al., 2020).

To also obtain information on past sea ice conditions at Site U1419, additional samples were studied for the sea ice diatom-derived monounsaturated highly branched isoprenoid IP_{25} (Belt et al., 2007). After adding 7-hexylnonadecane as internal standard, up to 6 g of sediment were extracted using an Accelerated Solvent Extractor (DIONEX, ASE 200; 100°C, 5 min, 1000 psi) with dichloromethane:methanol (2:1 v/v), and purified via open-column silica

chromatography (*n*-hexane). Identification and quantification of IP_{25} was achieved via coupled gas chromatography-mass spectrometry analyses following Müller et al. (2012).

3.5. Diatom analyses

After freeze-drying of sediments, samples were prepared following the acid-based method by Schrader & Gersonde (1978). Counts of identified species were carried out on permanent slides (Mountex® mounting medium). Several traverses across each slide were systematically tracked to obtain a representative count of valves (between 300 and 450 valves per slide). For the analysis of 251 samples we use a *Zeiss*® Axioscop with interference illumination (MARUM, University of Bremen). The counting of two replicate slides at x1000 magnification indicates an analytical error of ≤10.0 %. The census procedure and the definition of counting units followed standard methods (Schrader & Gersonde, 1978).

The resulting counts yielded relative abundance (%) of individual diatom taxa (determined as the fraction of the diatom species versus the total diatom concentration in a particular sample) as well as concentration of valves per g^{-2} (total diatom concentration), calculated as follows:

total diatom concentration = [N] x [A/a] x [1/W] x [V/v]

where, [N] number of valves in an known area [a], as a fraction of the total area of a petri dish [A], the sample weight [W] in g, and the final sample volume (V) and sample volume used for the permanent slide (v) (Sancetta & Calvert, 1988).

3.6. Coccolithophore abundance

Coccolithophore qualitative abundances range from barren to common (Jaeger et al., 2014a). Because of the wide range of abundances observed, we used a semi-quantitative methodology to capture the relative concentrations of coccolithophores in each sample. Strewn smear slides were made for 184 samples at ~40 cm resolution. Glass cover slips were adhered to the microscope slides using Norland Optical Adhesive No. 61. Total number of coccoliths per field of view (FOV) were recorded for 50 FOV per slide using a *Zeiss*® Axioscop A.1 at 1000x magnification. Abundance was recorded as the average number of coccoliths per FOV. While this method does not provide an accurate quantification of flux, it does reflect the relative shifts in high *vs* low coccolithophore content like qualitative scales (*e.g.*, Bottini & Erba, 2018; Guballa & Peleo-Alampay, 2020). The trends in coccolith FOV abundances follow the % carbonate curve, providing evidence that this method reflects the relative accumulation of coccoliths in sediments.

4. Results

4.1. Bulk sediment components

On average, bSi dominated the biogenic fraction of sediments at Site U1419 for the past 54 ka (Figure 2c). The contribution of bSi ranged between 0.1-39.8wt.% (average = 4.3±7.9). The contribution of $CaCO_3$ was 0.6-9.3% (average =2.4±1.0), and of TOC was 0.1-1.4% (average = 0.4±0.2).

Except for a few short intervals, values of bSi remained mostly below 5 wt.% (Figure 2c). The highest concentrations (14.0-39.0wt.%) were reached between 45.7 and 37.5 ka. A second highest maximum (33.8wt.%) occurred around 33.6 ka. The $CaCO_3$ concentration was higher between late MIS 3 and early MIS 1. Two maxima of $CaCO_3$ (7.3% and 9.2%) occurred at 21.23 and 34.83 ka. TOC values remained below 0.9 prior to 13 ka, increased abruptly at 12.5 ka and reached a maximum of 1.4% at 10.67 ka. From 10 ka to the present, TOC values decreased to less than 0.8% (Figure 2b). The concentrations of TOC and carbonate showed subtle increases associated with SE 1-4. Some maxima in $CaCO_3$ concentration roughly corresponded to SEs and high % carbonate intervals; however, there are exceptions to this trend.

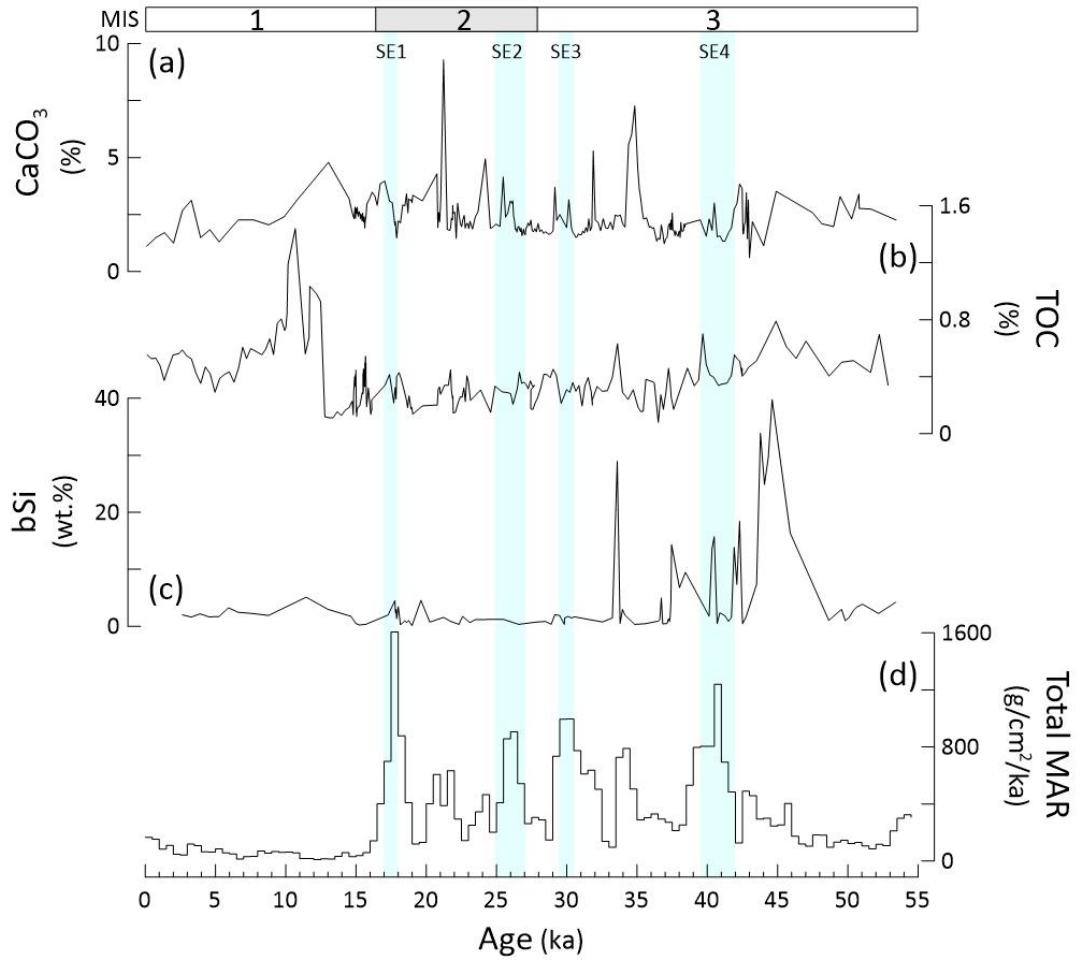

297 Figure 2. Concentration of bulk biogenic components (a-c) and total mass accumulation rate (MAR, d) at IODP Site U1419 for the past 54 ka. (a) $CaCO_3$ (%); (b) total organic carbon (TOC, %), (c) biogenic silica (bSi, wt.%) and (d) total MAR 300 ($g/cm^2/ka$) at Site U1419 for the past 54 ka. After Walczak et al. (2020), MAR is evaluated over constant timestep bins of 500 years to avoid interpretive artifacts associated with varying sample resolution. Light blue bars denote Siku Events (SE) 1-4 303 where IRD MAR exceeds 12 g cm^2 ka^{-1} (Walczak et al., 2020). MIS: Marine Isotope Stages.

4.2. Coccolithophorid components and alkenone concentration

306 Coccolith relative abundance ranged from barren (0 coccoliths/FOV) to 332 coccoliths/FOV with an average of 66.35 coccoliths/FOV. The highest abundances occurred during SE 4 (305 coccoliths/FOV), at ~14.5 ka (332 coccoliths/FOV, and at the beginning of 309 the Holocene (~9-10 ka; 209-246 coccoliths/FOV) (Figure 3a). Maxima in coccolith abundances roughly corresponded to SEs and high % carbonate intervals; however, there were exceptions to this trend.

312 The coccolithophore assemblage was dominated by *Coccolithus pelagicus* and *Geophyrocapsa muellerae*, both of which were found in high latitudes during the Quaternary (McIntyre & Be, 1967; Winter et al., 1994; Ziveri et al., 2004).

315 The $C_{37:2}$+$C_{37:3}$ alkenone concentrations ranged from 0.01 to 2.88 μg g^{-1} (Figure 3e). Maximum concentrations were recorded c. 48.3 ka (2.88 μg g^{-1}) and at 10.1-10.6 ka (1.94 μg g^{-1}), the latter peak marking a period of elevated alkenone concentrations during the
318 deglaciation (c. 9-11 ka). Overall, the lowest concentrations were recorded between 42-13 ka (<0.27 μg g^{-1}). There was no clear relationship between alkenone concentration and SEs.

4.3. Diatoms

321 #### 4.3.1. Concentration

The total diatom concentration varied strongly throughout the past 54 ka (range 0-8.3*10^6 valves gr^{-1}, average = 2.3*10^5 valves gr^{-1}±9.6*10^5). The occurrence of diatoms was
324 limited to a few intervals (Figure 3b). The highest concentration range (5.5-8.3*10^6 valves g^{-1}) was reached between 44.6 and 43.78 ka. A second highest maximum occurred around 33.6 ka.

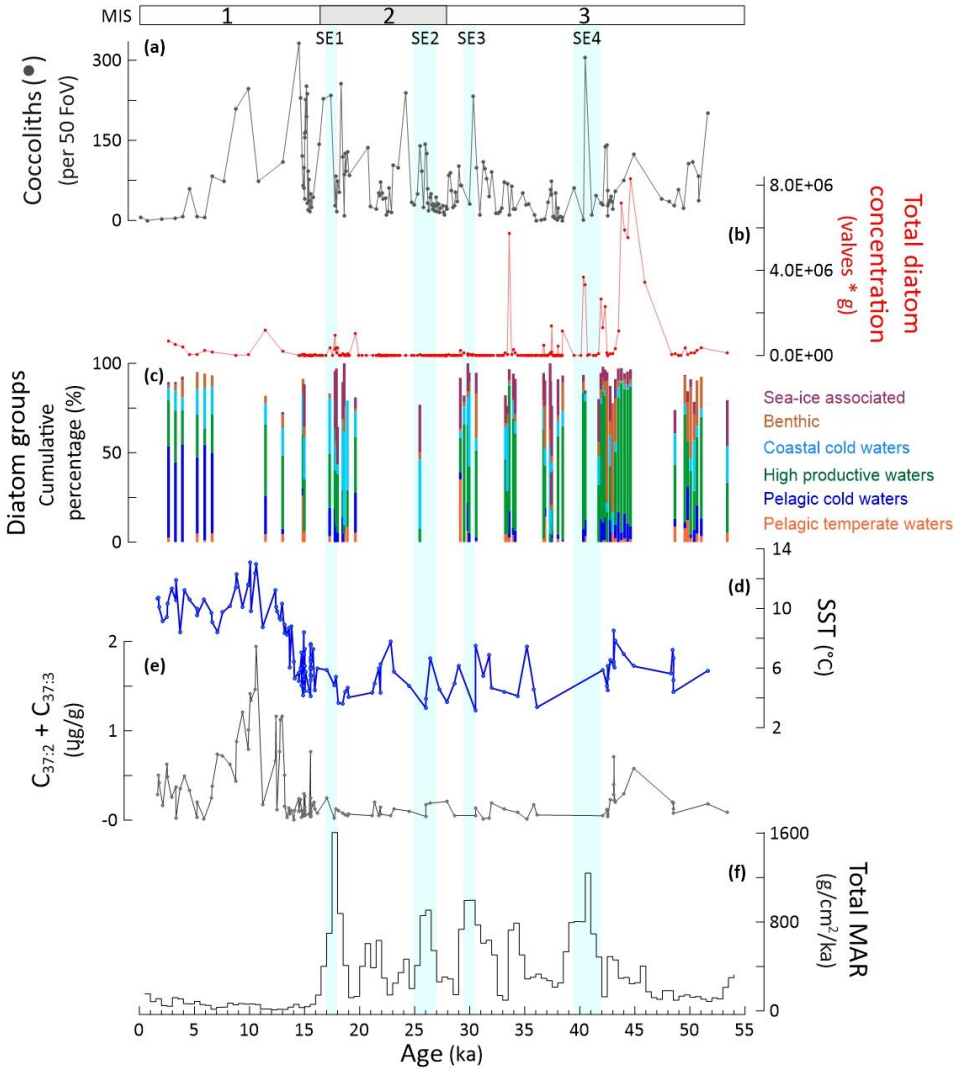

327

Figure 3. The productivity signal - Concentration of nannofossils and diatoms, the
330 composition of the diatom assemblage, reconstructed sea-surface temperature, and

$C_{37:2}$+$C_{37:3}$ and the total mass accumulation rate at IODP Site U1419 for the past 54 ka. (a) coccoliths (average per field of view - FoV), (b) total diatom concentration (valves g^{-2}, red line), (c) cumulative percentage of diatom groups (%, bars): sea-ice associated (crimson), benthic (red brown), coastal cold waters (light blue), high-productive waters (green), pelagic cold waters (dark blue), and pelagic temperate waters (orange) (for the composition of the diatom groups, see 4.3.2.); (d) $U^{K'}_{37}$ -based sea-surface temperature (SST, °C, blue line; calibrated using Müller et al., 1998), (e) $C_{37:2}$+$C_{37:3}$ (µg g^{-1}), and (f) total MAR (g cm^2 kyr^{-1}; from Walczak et al., 2020). The total MAR is evaluated over constant timestep bins of 500 years to avoid interpretive artifacts associated with varying sample resolution. Light blue bars denote Siku Events (SE) 1-4 where IRD MAR exceeds 12 g cm^2 ka (Walczak et al., 2020). MIS: Marine Isotope Stages.

4.3.2. Composition and temporal variation of diatom groups

Despite the sporadic occurrence of diatoms in Site U1419 sediments, the preserved diatom assemblage was diverse: up to 100 species occurred (Table 1, Supp. information). To better constrain the temporal occurrence of taxa, the 29 most abundant diatoms (averagely >0.75% of the entire record) were distributed in six groups. According to their ecology, groups represent the following environmental conditions/habitats: (1) sea-ice related, (2) benthic, (3) coastal cold waters, (4) high productive water, (5) pelagic cold water and (6) pelagic, temperate water diatoms. The species-specific composition of groups in given in Table S1.

(1) The most abundant **sea-ice related diatoms** at Site U1419 were spores and vegetative cells of *Thalassiosira antarctica*, *Bacterosira* spp., *Fragilariopsis cylindrus* and *Porosira glacialis* (Barron et al., 2009; Hasle & Syvertsen, 1996; Müller et al., 2018; Sancetta, 1981).

(2) *Paralia sulcata* dominated the **benthic** group. *Paralia sulcata* is a common component of the benthic and tycoplanktonic communities, thriving in shelf and uppermost slope waters along temperate to cool seas (Round et al., 1990). Secondary contributors to the benthic group were *Actinoptychus senarius*, *Actinoptychus vulgaris*, several species of *Cocconeis* and *Gomphonema*, *Delphineis kippae, Grammatophora marina*.

(3) Diatoms typically thriving in **cold coastal waters**, are today associated with low SST in oligo-to-mesotrophic waters with moderate to high dissolved silica levels, and became more abundant during intervals of weak turbulence (Crosta et al., 2012; Hasle & Syvertsen, 1996; Romero & Armand, 2010; Sancetta, 1981). Main components of this group were well-silicified *Shionodiscus trifulta, Shionodiscus oestrupii* var. *venrickae, Coscinodiscus oculus-iridis, Coscinodiscus argus, Cyclotella litoralis*, *Actinocyclus octonarius*, and *Thalassiosira gravida*.

(4) Several species of *Chaetoceros* resting spores (RS) and *Thalassionema nitzschioides* var. *nitzschioides* composed the **high-productive coastal water** group. Today, vegetative cells of numerous *Chaetoceros* species rapidly respond to the decay of upwelling intensity and nutrient depletion by forming endogenous resting spores (Hasle & Syvertsen, 1996). Spores of *Chaetoceros* and *T. nitzschioides* var. *nitzschioides* are common components of the upwelling assemblage in low- and high-latitude coastal areas (Nave et al., 2001; Romero & Armand, 2010; Romero et al., 2021).

(5) Diatoms occurring in **pelagic cold waters**, which today mainly respond to low-to-moderate DSi content in hemi-to-pelagial waters of moderate to low SST (Barron et al., 2009; Hasle & Syvertsen, 1996; Sancetta, 1981). *Neodenticula seminae* and *Thalassiosira nordenskioldii* contributed the most to this group at Site U1419.

(6) The assemblage typical of **pelagic temperate waters** was composed of taxa, which today thrive in open-ocean temperate waters, with low to moderate levels of DSi levels and weak mixing (Crosta et al., 2012; Nave et al., 2001; Romero et al., 2005, 2021). At Site U1419, this group was dominated by *Roperia tesselata* and *Stephanopyxis* spp.

Each group contributed averagely as follows: (1) sea-ice related = 10.93±9.88%, (2) benthic = 8.99±12.99%, (3) cold coastal waters = 14.26±13.78%, (4) high coastal productive waters = 39.51±21.88%, (5) pelagic cold waters = 11.06±13.82% and (6) pelagic temperate waters = 3.10±5.12% (sum of the averages = 87.85%). Due to the low occurrence of valves in several samples, we present data of the relative contribution (%) of each group only for a minor number of counted samples (Figure 3c). The six diatom groups showed a clear temporal pattern. Diatoms typical of high productive coastal waters were the main contributors to the highest maxima of diatom concentration/MAR, mainly between 54 and 29 ka (early – late MIS 3) (Figure 3c). A shift in the composition of the community occurred after 29 ka onto younger times (roughly the MIS 3/2 boundary). Coastal cold water and sea-ice related diatoms were dominant between 29 and 17 ka (begin of the deglaciation). The last deglacial showed a diverse diatom assemblage, without a particular group being dominant. Diatoms typical of cold and temperate pelagic waters dominated during the Holocene (10 – 2 ka).

4.4. SST

$U_{37}^{K'}$-based SSTs ranged from ~3 to 13°C (Figure 3d). Since modern surface sediments in the GoA suggest a summer bias to the $U_{37}^{K'}$ proxy (Méheust et al., 2013; Prahl et al., 2010;

Tierney & Tingley, 2018), we interpreted these data to reflect summer SSTs. Overall, SSTs remained low (~6°C) over the glacial period (MIS3 and MIS2). Unfortunately, there were no data available for SE 4. The onset of each following SE event (SE3, SE2, SE1), however, seemed to be accompanied by a short-term drop in SST, which was immediately followed by a slight warming trend. There were also minor millennial scale variations in SST which do not align with the SE events throughout the glacial stage. A more significant warming occurred during the deglaciation from 14.5-10.3 ka. SSTs increased more rapidly after 13.8 ka and remained above 8.5°C for most of the Holocene. Holocene SSTs oscillated between 8-13°C, in contrast to the SSTs of ~3-9°C prior to 15 ka.

4.5. Sea-ice markers

Concentrations of the spring sea-ice biomarker IP_{25} exhibited significant fluctuations over the studied sediment interval with IP_{25} mainly absent between 55 ka and 42 ka as well as during some short intervals at ca. 38 ka, 30 ka, 16 ka and throughout the Holocene (Figure 4a). Elevated concentrations (0.6 - 2.4 µg/g) were observed during SE 4, at about 32 and 27 ka, between 25 and 19 ka and at about 14 ka. $C_{37:4}$ concentration maxima occurred before 14 ka, and decline between 14-6 ka, although there were also intervals of exceptionally low $C_{37:4}$ concentrations throughout the record. While we note similarities between the general IP_{25} pattern and $C_{37:4}$ abundances, a distinct relation between IP_{25} and $C_{37:4}$ concentrations and SE events, was not discernable.

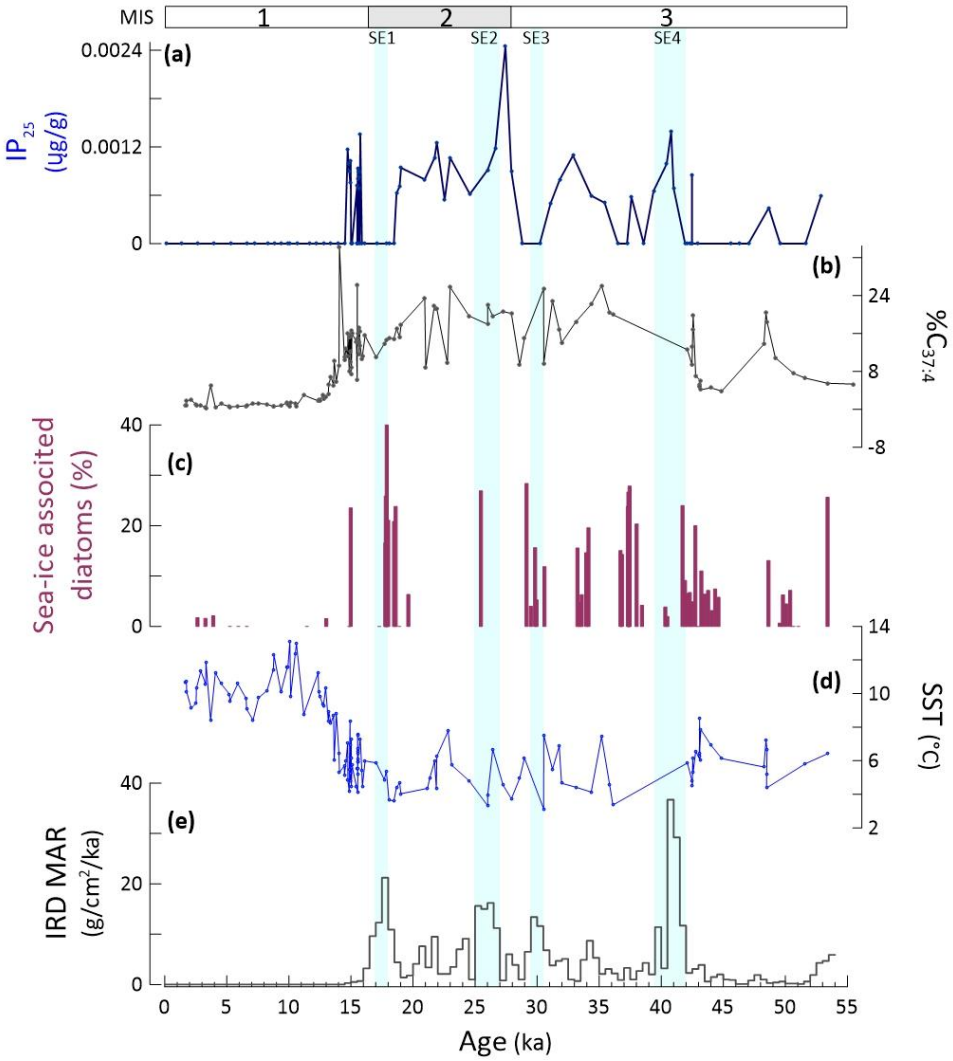

420 Figure 4. The sea ice signal - Concentration of biomarkers and sea-ice associated diatoms, sea-surface temperature (SST) and mass accumulation rate of ice-rafted debris (IRD MAR) at IODP Site U1419 for the past 54 ka. (a) IP_{25} (μg g^{-2}), (b) $\%C_{37:4}$
423 alkenone, (c) sea-ice associated diatoms (relative contribution of the total diatom assemblage, %), (d) $U^{K'}_{37}$ -based sea-surface temperature (SST, °C), and (e) IRD MAR (g cm^2 ka^{-1}; from Walczak et al., 2020). The IRD MAR is evaluated over constant timestep
426 bins of 500 years to avoid interpretive artifacts associated with varying sample resolution. Light blue bars denote Siku Events (SE) 1-4 where IRD MAR exceeds 12 g cm^2 ka (Walczak et al., 2020). MIS: Marine Isotope Stages.

429

5. Discussion

The long-term temporal evolution of reconstructed productivity, sea surface conditions
432 (SST, sea ice cover) and iceberg discharge at Site U1419 for the last 54 ka followed a glacial-interglacial pattern of variability. High concentrations of $CaCO_3$, coccolithophorids, bSi, and diatoms mostly occurred in MIS 3 (54-28 ka) and MIS 2 (28-17.3 ka). TOC values remained
435 below 0.8% and $C_{37:2}$ + $C_{37:3}$ alkenones below 1 μg g^{-1} until ca. 13 ka, then abruptly increased at 12.5 ka (Figures 2b, 3e). SSTs were low from MIS 3 until ca. 14 ka, and increased into the

Holocene (Figures 3d, 4d). Although sea ice biomarkers (IP_{25} and $C_{37:4}$) and the sea-ice
438 associated diatoms showed variable signals, they were predominantly present during MIS 3 and MIS 2 and decreased from 14.5 ka in line with increasing SSTs (Figures 3d, 4a, d). Superimposed on these orbital-paced variations, some proxies at Site U1419 showed
441 suborbital-scale variations of diverse amplitude.

5.1. Productivity and sea-surface conditions in the northern GoA from MIS 3 through MIS 2 (54 – 17.3 ka): impact of icebergs and meltwater discharge

444 Located in an HNLC region of the northeastern coastal Pacific Ocean (Childers et al., 2005), Site U1419 underlies surface waters known to be largely iron-limited (Boyd et al., 2007; Martin, 1990). We argue that iron limitation largely defined the pattern of
447 phytoplankton occurrence and the productivity in surface waters of the northern GoA during the past 54 ka.

The present-day iron limitation in the GoA affects the composition and dynamics of the
450 phytoplankton communities (Childers et al., 2005; Strom et al., 2006, 2016). *In situ* iron enrichments of surface ocean waters of the GoA result in diatom blooms, demonstrating that phytoplankton growth in HNLC waters is controlled by the iron supply (Boyd et al.,
453 2004, 2007). Since the magnitude of iron input to high-latitude oceans has changed over geological timescales (Martínez-García et al., 2011; Müller et al., 2018), it is essential to reassess its possible impact on past dynamics of primary producers. Possible mechanisms
456 responsible for iron delivery to GoA surface waters between 54 and 17.3 ka might have been: (*i*) meltwater discharge from the northern CIS (Addison et al., 2012; Cowan et al., 2020), (*ii*) seasonal mixing of the uppermost water column (Crusius et al., 2011), (*iii*) aeolian
459 input, and (*iv*) eddy-mediated offshore transport of coastal waters (Crusius et al., 2017). Although these mechanisms might have impacted primary productivity in different ways throughout the studied interval, we assign a major role of surface water fertilization to iron
462 delivery via iceberg and meltwater discharges from tidewater termini (Cowan et al., 2020; Crusius et al., 2017). Site U1419 was drilled on the Alaskan continental shelf, ca. 30 km west of the Bering Trough mouth (Jaeger et al., 2014a). This shelf-crossing trough was occupied by
465 the Bering icestream at the Last Glacial Maximum (Cowan et al., 2020; Figure 1). Because of the study site's proximity to the Bering icestream (Figure 1), we propose that the occurrence of the highest bulk biogenic and microfossil concentrations between mid MIS 3 (45 ka) and
468 late MIS 2 (17.3 ka, shortly before the start of the last deglaciation) were due to tidewater

glacier-mediated discharges of sediment-laden (iron bearing) meltwater and icebergs from the northern CIS (Penkrot et al., 2018).

Diatom and - to a lesser extent - coccolithophorid occurrence at Site U1419 was mostly confined to short-lived events between mid MIS 3 and early MIS 1 (45-13 ka). Although abundance values were generally low, coccolithophorids were more commonly present than diatoms throughout the Site U1419 record (Figure 3a-c). Differences noted in the temporal pattern of $CaCO_3$ and bSi concentration (Figure 2) were evident in the record of coccolithophorids and diatoms. Differences in the timing of siliceous and calcareous occurrence in the northern GoA for the past 54 ka are thus more likely to reflect the differential response of diatoms and coccolithophores to (*i*) available nutrient pools, (*ii*) the main season of production for each phytoplankton group and/or (*iii*) the response to dissolution throughout the water column and at the water-sediment interface. Presently, diatoms dominate the spring phytoplankton bloom in the GoA, while coccolithophores dominates the late summer-fall phytoplankton bloom (Childers et al., 2005; Stabeno et al., 2004). However, modern studies in the GoA have been unable to link diatom (Strom et al., 2006) or coccolithophore (Lipsen et al., 2007) productivity to one single factor such as irradiance or nutrient limitation, indicating a complex oceanographic and biogeochemical system (Childers et al., 2005). The alignment of coccolithophore abundance peaks and, to a lesser extent, bSi (=diatom) concentration, with SEs (Figure 3a, b) suggests that the phytoplankton production was linked to enhanced nutrient availability during glacial outflow events on geological time scales. In turn, the good match between these episodes of phytoplankton productivity and the concentration of bulk biogenic components indicates that coccolithophores and diatoms largely contributed to the $CaCO_3$ and bSi (and TOC) flux in the northern GoA.

In addition to productivity, the concentration of bulk sediment components, fossil records, and biomarkers could be influenced by preservation or source. Carbonate dissolution can occur in waters that are oversaturated with respect to calcium carbonate because of the respiration of organic carbon in the water column and at the water/sediment interphase (Wollast & Chou, 1998). Organic carbon preservation is enhanced with high sediment burial rates or low oxygen water conditions (Canfield, 1994). Despite the increase in carbonate and TOC MAR during the SEs (Supp. information), the concentrations did not vary greatly over the study interval (Figure 2), suggesting that there was a steady flux of

carbon being preserved in the sediments of the northern Alaskan slope independent of glacial outflow events. The MAR maxima during the SEs could also be influenced by an increase in terrestrially derived material. Terrestrial aquatic ratio (TAR) values, however, indicate that the organic matter preserved during these intervals was of marine origin (Supp. information). Accumulation of terrestrial carbonate cannot be ruled out.

A prominent feature of the primary producers' record is their asynchronous pattern of occurrence. Although different rates of preservation could be a factor for biogenic components, we observe similarities between concentrations of both inorganic and organic components for our phytoplankton groups (*e.g*. nannofossil counts and $C_{37:2}$+$C_{37:2}$ alkenones; Figure 3a, e), which are unlikely to have been driven by the same preservation factors (*e.g*., water column or sediment oxygenation for organic matter, dissolution processes for inorganic constituents). For example, the large peak in bSi and to a lesser extent in TOC at ~45-50 ka (Figure 2b, c) occurred alongside a low-oxygen event identified at Site U1419 (Sharon et al., 2021; Zindorf et al., 2020), but these conditions should not have impacted the preservation of siliceous organisms (Nelson et al., 1995). Rather, a high flux of biogenic components (especially TOC) to the seafloor at this time is more likely to have driven the generation of low-oxygen conditions as organic matter was respired.

Since the mean value of SST remained mostly below 8°C between 54 and 17.3 ka, and no significant shift between cooling and warming occurred during intervals of high coccolithophorid and/or diatom production (Figure 3), we argue that the occurrence of siliceous and calcareous primary producers was unaffected by low SST conditions during MIS 3 and MIS 2 in the northern GoA. Although the match between the sporadic occurrence of diatoms and SST variations was not consistent over the interval 54-17.3 ka, the long-term SST dynamics appear to have determined the changes in composition of the diatom community. The dominance of diatoms typical of cold and high productive coastal waters between 54 and 17.3 ka (Figure 3c) matched the generally low SSTs (Figure 3d) and spring sea ice occurrences indicated by IP_{25} (Figure 4d). However, spring sea ice cover seems to have exerted no major control on coccolithophore productivity either but potentially limited diatom growth (except for SE 4) as the total diatom concentration was low overall after 39 ka (*i.e*., since IP_{25} and $C_{37:4}$ abundances point to the recurring presence of spring sea ice cover at Site U1419, Figure 4a, b).

CIS outlet glaciers along the Alaskan coast terminated with a grounded tidewater terminus, thus they slowly advanced over the course of centuries, until thinning initiated a rapid retreat that was completed within decades, stabilizing when the glacier reached shallow water depths (Cowan et al., 2020, and references therein). Once tidewater glacier retreat was initiated, the glacier's behavior was only weakly influenced by climate (*e.g.*, SST, Pfeffer, 2007), and trough geometry and sea level primarily controlled terminus behavior (Enderlin et al., 2013). The pattern of SST variability at Site U1419 provide further evidence of the CIS controlling the coastal regime dynamics. SST variability was not always in phase with iceberg discharges as colder SSTs were not always linked to SEs (*e.g.*, low SSTs at 32 ka and 37 ka, between SE 4 and SE 3, Figure 3d).

5.2. SST warming, decrease of bioavailable iron and weakened productivity between the last deglacial and late Holocene (17.3-2 ka)

The abrupt decrease of MAR at Site U1419 around 17.3 ka (Figure 2d) signaled the early stages of glaciers' stagnation or retreat into the last deglaciation (Cowan et al., 2020). The long-term glaciers' retreat and the sea level increase associated with the last deglacial led to a flooding of the coastal plains along northern Alaska. Remobilized iron originated from the newly inundated Alaskan shelf might have fueled primary productivity events after the LGM and in turn contributed to sedimentary anoxia (Davies et al., 2011; Sharon et al., 2021; Zindorf et al., 2020). While sea ice indicators then return to zero and SSTs reach maximum values at 10 ka, highest TOC contents and elevated $C_{37:2}$+$C_{37:3}$ concentrations (Figures 2d, 3e) are observed between 13 -10 ka at Site U1419 (Figure 2b). This observation is in line with a widespread phenomenon along the Alaskan margin during the last deglaciation (Addison et al., 2012; Barron et al., 2009; Davies et al., 2011), and provides additional evidence of higher productivity due to the sudden fertilization of surface coastal waters. Regarding the low MAR during this interval, we conclude that the transport of terrigenous organic matter from Alaska (Figure S2) carried by meltwater can be ruled out as a driver for this TOC maximum as this would have caused an increase in the sedimentation rate (and an elevated MAR; Figures 2, S2).

There is a noticeable millennial-scale variability of SST superimposed on a significant warming trend between 16 and 10 ka, which is accompanied by short-term fluctuations and an overall decrease in the abundance of IP_{25} and $C_{37:4}$ until 13 ka (Figure 4). These rapid variations suggest that a readvance of sea ice coverage developed, perhaps in response to

564 meltwater discharge from retreating glaciers. In line with the SST warming during the last deglacial, an increase in the contribution of diatoms thriving in more temperate waters occurred between 15 and 10 ka, with lessened contribution of cold and high productive
567 coastal waters (unfortunately only four samples with a statistically significant number of valves can be considered; Figure 3c). Similar observations on the shift of diatom species composition are known for the nearby core EW0408-85CJ (Barron et al., 2009).

570 The overall low IRD after 15 ka followed the glacier retreat scenario coupled with SST warming (confirming the trend observed at Site U1419 in the site survey core by Praetorius et al., 2015), a highly stratified uppermost water column (Royer & Grosch, 2006), and
573 weakened iceberg-mediated iron fertilization of the ocean surface. An increasingly stratified uppermost water column during the Holocene led to (*i*) the decreased resuspension of sediments, as well as (*ii*) the reduction of iron delivery into shelf waters (Crusius et al., 2017).
576 The Holocene as preserved at Site U1419 recorded only minor environmental changes. The only striking productivity events were the peaks in coccolith, $C_{37:2}$+$C_{37:3}$ alkenone concentrations and TOC% between 10 and 8.5 ka (Figure 3b; not shown in total MAR, Figure
579 2a, see also Supp. information), which occurred alongside SST maxima. Surface waters overlying Site U1419 then gradually cooled to 8°C until 7 ka, followed by warming through the late Holocene (8.5-11°C, Fig 3d). The higher contribution (50-55%) of diatoms typical of
582 pelagic temperate and cold waters after 7 ka matches well the warming recorded by the $U_{37}^{K\prime}$-based temperatures (Figure 3c, d) and the lowered surface water production (Barron et al., 2009). The Site U1419 record displayed no indication of significant CIS discharge after 7
585 ka.

With decreased extension of the CIS after the last deglaciation, other mechanisms of iron delivery might have become more important. Local sources of dust include extensive areas
588 along the southern Alaskan coastline where the glacier melting season lasts several months (Neal et al., 2010), exposing dust in glacierized river valleys (Crusius et al., 2011) which can then be carried over hundreds of kilometers beyond the shelf break in late autumn dust
591 storms (Crusius et al., 2011; Schroth et al., 2017). Following present-day analogues (Crusius et al., 2011, 2017), we propose that vast areas in Alaska became more active sources of dust for bioavailable iron after the last deglaciation throughout the late Holocene. However, their
594 impact on primary producers seems to be less crucial beyond the Alaskan continental shelf,

since - except for the coccolithophorid maximum between 10 and 8 ka - primary producers' values resemble those recorded before the Holocene.

6. CONCLUSIONS

Our multiproxy assessment combines for the first time the study of siliceous and calcareous microfossils, bulk biogenic components, biomarkers, and ice-rafted debris for the reconstruction of sea-surface conditions, and sea ice occurrence at IODP Site U1419 off Alaska for the past 54 ka. This multiproxy approach allows us to investigate the forcings driving paleoenvironmental change of upper ocean properties in the high-latitude northeastern Pacific on orbital and suborbital timescales.

Collapse of the CIS and the associated meltwater discharge actively defined both the orbital and suborbital timescales of productivity and sea-surface oscillations in the northern GoA. Bioavailable iron (mainly linked to iceberg discharge) largely controlled the pattern of primary productivity occurrence in waters overlying Site U1419.

The occurrence of siliceous and calcareous primary producers at Site U1419 is not consistently linked with SST variability over the entire record. SST changes were not linked to marine producers' dynamics on the suborbital timescale during MIS 3 and MIS 2, suggesting that SST is not a primary forcing of productivity change on these timescales.

Despite minor productivity peaks, less favorable conditions for primary producers prevailed between the last deglaciation (17-11 ka) and the late Holocene. Compared to MIS3 and MIS2, the significant reduction of CIS cover after the last deglaciation and weakened meltwater discharge into the northern GoA negatively impacted productivity in surface waters overlying the Alaskan slope.

Our multiproxy reconstruction suggests that iron fertilization actively fueled primary productivity in the HNLC waters adjacent to Alaskan continental ice sheets during the Late Pleistocene. This study supports the scenario of the GoA representing an ice-proximal marine environment where primary productivity, and potentially also CO_2 draw-down, are closely linked to ice-sheet dynamics (Martin, 1990).

ACKNOWLEDGMENTS

We thank the Integrated Ocean Drilling Program U.S. Implementing Organization (IODP-USIO) and the captain and crew of the D/V *JOIDES Resolution* during Expedition 341. This

research used samples provided by the IODP. Funding was provided by the German Research Foundation (DFG) (RO3039/4, and MU3670/1-2), the Helmholtz Association (VH-NG-1101), the Philip Leverhulme Prize (ELM), and a NERC-IODP grant (NE/L002426/1, ELM), a US Science Support Program Post-Expedition Activity award to LJL. LJL's salary is provided through NSF award OCE-1326927. LJL thanks C. Ramsey and D. Mmasa for their work collecting coccolith counts. Funding was provided by the National Science Foundation award OCE-1434945 and a post-expedition award from the U.S. Science Support Program of IODP to EAC.

Data Availability Statement

Data files are archived at https://doi.pangaea.de/10.1594/PANGAEA.932584.

7. REFERENCES

Addison, J. A., Finney, B.P., Dean, W.E., Davies, M.H., Mix, A.C., Stoner, J.S., & Jaeger, J.M. (2012). Productivity and sedimentary $\delta^{15}N$ variability for the last 17,000 years along the northern Gulf of Alaska continental slope. *Paleoceanography*, 27(1). 10.1029/2011pa002161.

Barron, J. A., Bukry, D., Dean, W.E., Addison, J. A., & Finney, B. (2009). Paleoceanography of the Gulf of Alaska during the past 15,000 years: Results from diatoms, silicoflagellates, and geochemistry. *Marine Micropaleontology*, 72(3), 176-195.

Belt, S. T., Massé, G., Rowland, S. J., Poulin, M., Michel, C., and LeBlanc, B. (2007). A novel chemical fossil of palaeo sea ice: IP_{25}. *Organic Geochemistry*, 38, 16-27.

Blain, S., Quéguiner, B., Armand, L., Belviso, S., Bombled, B., Bopp, L., et al. (2007). Effect of natural iron fertilization on carbon sequestration in the Southern Ocean. *Nature,* 446(7139), 1070-1074.

Bottini, C., & Erba, E. (2018). Mid-Cretaceous paleoenvironmental changes in the western Tethys. *Climate of the Past*, 14, 1147-1163. https://doi.org/10.5194/cp-14-1147-2018

Boyd, P. W., Jickells, T., Law, C. S., Blain, S., Boyle, E. A., Buesseler, K. O., et al. (2007). Mesoscale Iron Enrichment Experiments 1993-2005: Synthesis and Future Directions. *Science*, 315(5812), 612-617.

Boyd, P. W., & Ellwood, M. J. (2010). The biogeochemical cycle of iron in the ocean. *Nature Geoscience*, 3(10), 675-682, 10.1038/ngeo964

Canfield, D.E. (1994). Factors influencing organic carbon preservation in marine sediments. *Chemical Geology*, 114(3-4), 315-329. https://doi.org/10.1016/0009-2541(94)90061-2

Childers, A. R., Whitledge, T. E., & Stockwell, D.A. (2005). Seasonal and interannual variability in the distribution of nutrients and chlorophyll a across the Gulf of Alaska shelf: 1998–2000. *Deep Sea Research II*, 52(1), 193-216.

Cowan, E. A., Zellers, S. D., Müller, J., Walczak, M. H., Worthington, L.L., Caissie, B. E., et al. 2020. Sediment controls dynamic behavior of a Cordilleran Ice Stream at the Last Glacial Maximum. *Nature Communications*, 11(1), 1826. DOI: 10.1038/s41467-020-15579-0

Coyle, K.O., Hermann, A.J., & Hopcroft, R.R. (2019). Modeled spatial-temporal distribution of productivity, chlorophyll, iron and nitrate on the northern Gulf of Alaska shelf relative to field observations. *Deep-Sea Research Part II*, 165, 163-191. https://doi.org/10.1016/j.dsr2.2019.05.006

Crawford, W. R., Brickley, P. J., & Thomas, A. C. (2007). Mesoscale eddies dominate surface phytoplankton in northern Gulf of Alaska. *Progress in Oceanography*, 75(2), 287-303.

Crosta, X., Romero, O. E., Ther, O. & Schneider, R. R. (2012). Climatically-controlled siliceous productivity in the eastern Gulf of Guinea during the last 40 000 yr. *Climate of the Past*, 8(2), 415-431. 10.5194/cp-8-415-2012

Crusius, J., Schroth, A. W., Gassó, S., Moy, C. M., Levy, R. C., & Gatica, M. (2011). Glacial flour dust storms in the Gulf of Alaska: Hydrologic and meteorological controls and their importance as a source of bioavailable iron. *Geophysical Research Letters*, 38(6), https://doi.org/10.1029/2010GL046573

Crusius, J., Schroth, A. W., Resing, J. A., Cullen, J., & Campbell, R. W. (2017). Seasonal and spatial variabilities in northern Gulf of Alaska surface water iron concentrations driven by shelf sediment resuspension, glacial meltwater, a Yakutat eddy, and dust. *Global Biogeochemical Cycles*, 31(6), 942-960.

Davies, M. H., Mix, A. C., Stoner, J. S., Addison, J. A., Jaeger, J., Finney, B., & Wiest. J. (2011), The deglacial transition on the southeastern Alaska Margin: Meltwater input, sea level rise, marine productivity, and sedimentary anoxia, *Paleoceanography*, 26, PA2223, doi:10.1029/2010PA002051

Duprat, L. P. A. M., Bigg, G. R., & Wilton, D. J. (2016). Enhanced Southern Ocean marine productivity due to fertilization by giant icebergs. *Nature Geoscience*, 9(3), 219-221.

Enderlin, E. M., Howat, I. M., & Vieli, A. (2013). High sensitivity of tidewater outlet glacier dynamics to shape. *The Cryosphere*, 7, 1007–1015, https://doi.org/10.5194/tc-7-1007-2013.

Freeland, H. J. (2006). What proportion of the north pacific current finds its way into the Gulf of Alaska?, *Atmosphere-Ocean*, 44, 321-330, DOI: 10.3137/ao.440401

Guballa, J. D. S., & Peleo-Alampay, A. M. (2020). Pleistocene calcareous nannofossil biostratigraphy and gephyrocapsid occurence in Site U1431D, IODP 349, South China Sea. *Geosciences*, 10, 388. https://doi.org/10.3390/geosciences10100388

Halse, G. R., & Syvertsen, E. E. (1996). Marine Diatoms. In C. R. Tomas, *Identifying Marine Diatoms and Dinoflagellates* (pp. 5-385). San Diego, Academic Press. https://doi.org/310.1016/B1978-012693015-012693013/012650005-X

Haslett, J., & Parnell, A. (2008). A simple monotone process with application to radiocarbon-dated depth chronologies. *Journal of the Royal Statistical Society: Series C (Applied Statistics)*, 57, 399–418. doi:10.1111/j.1467-9876.2008.00623.x

Henson, S.A. (2007). Water column stability and spring bloom dynamics in the Gulf of Alaska. *Journal of Marine Research*, 65(6), 715-736. https://doi.org/10.1357/002224007784219002

Hopwood, M. J., Bacon, S., Arendt, K., Connelly, D. P., & Statham, P. J. (2015). Glacial meltwater from Greenland is not likely to be an important source of Fe to the North Atlantic. *Biogeochemistry*, 124(1), 1-11.

Jaeger, J. M., Gulick, S. P. S., LeVay, L. J., & the Expedition 341 Scientists (2014a) *Proceedings of the Integrated Ocean Drilling Program*, 341. College Station, Texas, Integrated Ocean Drilling Program, https://doi .org /10 .2204 /iodp.proc.341.101.2014

Jaeger, J. M., Gulick, S. P. S., LeVay, L. J., Asahi, H., Bahlburg, H., Belanger, C. L., Berbel, G. B. B., Childress, L. B., Cowan, E. A., Drab, L., Forwick, M., Fukumura, A., Ge, S., Gupta, S. M., Kioka, A., Konno, S., März, C. E., Matsuzaki, K. M., McClymont, E. L., Mix, A. C., Moy, C. M., Müller, J., Nakamura, A., Ojima, T., Ridgway, K. D., Rodrigues Ribeiro, F., Romero, O. E., Slagle, A. L., Stoner, J. S., St-Onge, G., Suto, I., Walczak, M. H., and Worthington, L. L. (2014b) Methods. *In* Jaeger, J. M., Gulick, S. P. S., LeVay, L. J., and the Expedition 341 Scientists, *Proc. IODP*, 341: College Station, TX (Integrated Ocean Drilling Program). doi:10.2204/iodp.proc.341.102.2014

Kim, J.-H., Schneider, R. R., Müller, P. J., & Wefer, G. (2002). Interhemispheric comparison of deglacial sea-surface temperature patterns in Atlantic eastern boundary currents. *Earth and Planetary Science Letters*, 194(3), 383-393, https://doi.org/310.1016/S0012-1821X(1001)00545-00543

Kipphut, G. W. (1990). Glacial Meltwater Input to the Alaska Coastal Current: Evidence from Oxygen Isotope Measurements. *Journal of Geophysical Research: Oceans*, 95(C4), 5177-5181.

Lipsen, M. S., Crawford, D. W., Gower, J., & Harrison, P. J. (2007). Spatial and temporal variability in coccolithophore abundance and production of PIC and POC in the NE subarctic Pacific during El Niño (1998), La Niña (1999) and 2000. *Progress in Oceanography*, 75(2), 304-325. doi.org/10.1016/j.pocean.2007.08.004

Martin, J. H. (1990). Glacial-interglacial CO_2 change: The iron hypothesis. *Paleoceanography*, 5, 1–13.

Martínez-García, A., Rosell-Melé, A., Jaccard, S. L., Geibert, W., Sigman, D. M., & Haug, G. H. (2011). Southern Ocean dust–climate coupling over the past four million years. *Nature*, 476(7360), 312-315. 310.1038/nature10310.

McIntyre, A., & Be, A. W. H. (1967). Modern coccolithophoridae oft he Atlantic Ocean – I. Placoliths and cyrtoliths. *Deep Sea Research and Oceanographic Abstracts*, 14(5), 561-597. https://doi.org/10.1016/0011-7471(67)90065-4

Méheust, M., Fahl, K., & Stein, R. (2013). Variability in modern sea surface temperature, sea ice and terrigenous input in the sub-polar North Pacific and Bering Sea: Reconstruction from biomarker data. *Organic Geochemistry*, 57, 54-64. https://doi.org/10.1016/j.orggeochem.2013.01.008

Müller, P.J., & Schneider, R. R. (1993). An automated leaching method for the determination of opal in sediments and particulate matter. *Deep-Sea Research Part I*, 40, 425-444.

Müller, P.J., Kirst, G., Ruhland, G., von Storch, I., & Rosell-Mellé, A. (1998). Calibration of the alkenone palaeotemperature index UK-37 based on core-tops from the eastern South Atlantic and the global ocean (60°N–60°S). *Geochimica et Cosmochimica Acta*, 62, 1757–1772.

Müller, J., Werner, K., Stein, R., Fahl, K., Moros, M., & Jansen, E. (2012). Holocene cooling culminates in sea ice oscillations in Fram Strait. *Quaternary Science Reviews*, 47, 1-14.

Müller, J., Romero, O. E., Cowan, E. A., McClymont, E. L., Forwick, M., Asahi, H., et al. (2018). Cordilleran ice-sheet growth fueled primary productivity in the Gulf of Alaska, northeast Pacific Ocean. *Geology*, 46(4), 307-310, https://doi.org/10.1130/G39904.1

Nave, S., Freitas, P., & Abrantes, F. (2001). Coastal upwelling in the Canary Island region: spatial variability reflected by the surface sediment diatom record. *Marine Micropaleontology*, 42(1), 1-23. https://doi.org/10.1016/S0377-8398(1001)00008-00001

Neal, E. G., Hood, E., & Smikrud, K. (2010). Contribution of glacier runoff to freshwater discharge into the Gulf of Alaska. *Geophysical Research Letters*, 37(6), L06404, doi:10.1029/2010GL042385.

Nelson, D. M., Tréguer, P., Brzezinski, M. A., Leynaert, A., & Quéguiner, B. (1995). Production and dissolution of biogenic silica in the ocean: Revised global estimates, comparison with regional data and relationship to biogenic sedimentation. *Global Biogeochemical Cycles* 9(3), 359-372.

Penkrot, M. L., Jaeger, J. M., Cowan, E. A., St-Onge, G., & LeVay, L. (2018). Multivariate modeling of glacimarine lithostratigraphy combining scanning XRF, multisensory core properties, and CT imagery: IODP Site U1419. *Geosphere*, 14(4), 1–26, https://doi.org/10.1130/GES01635.1.

Pfeffer, W. T. (2007) A simple mechanism for irreversible tidewater glacier retreat. *Journal of Geophysical Research Earth Surface*, 112(F3): F03S2. DOI: 10.1029/2006JF000590

Praetorius, S. K., Mix, A. C., Walczak, M. H., Wolhowe, M. D., Addison, J. A., & Prahl, F. G. (2015). North Pacific deglacial hypoxic events linked to abrupt ocean warming. *Nature*, 527(7578), 362-366.

Praetorius, S. K., Rugenstein, M., Persad, G., & Caldeira, K. (2018). Global and Arctic climate sensitivity enhanced by changes in North Pacific heat flux. *Nature Communications*, 9(1), 3124.

Prahl, F. G., & Wakeham, S. G. (1987). Calibration of unsaturation patterns in longchain ketone compositions for paleotemperature assessment. *Nature*, 330, 367–369.

Prahl F. G., Muelhausen L. A., & Zahnle D. L. (1988) Further evaluation of long-chain alkenones as indicators of paleoceanography conditions. *Geochimica et Cosmochimica Acta*, 52, 2303–2310.

Prahl, F. G., Rontani, J.-F., Zabeti, N., Walinsky, S. E., & Sparrow, M.A. (2010). Systematic pattern in U37K′-temperature residuals for surface sediments from high latitude and other oceanographic settings. *Geochimica et Cosmochimica Acta*, 74, 131–143.

Reimer, P. J., Bard, E., Bayliss, A., Beck, J. W., Blackwell, P. G., Ramsey, C. B., Buck, C. E., et al. (2013). IntCal13 and Marine13 Radiocarbon Age Calibration Curves 0–50,000 Years cal BP. *Radiocarbon,* 55, 1869–1887 (2013). doi:10.2458/azu_js_rc.55.16947

Romero, O. E., Armand, L. K., Crosta, X., & Pichon, J. J. (2005). The biogeography of major diatom taxa in Southern Ocean surface sediments: 3. Tropical/Subtropical species. *Palaeogeography, Palaeoclimatology, Palaeoecology*, 223(1), 49-65.

Romero, O. E., & Armand, L. K. (2010). Marine diatoms as indicators of modern changes in oceanographic conditions. In: Smol, J. P., Stoermer, E. F. (Eds.), *The Diatoms, Applications for the Environmental and Earth Sciences* (Second Edition (pp. 373-400). Cambridge University Press, Cambridge.

Romero, O. E., Ramondenc, S., & Fischer, G. (2021). A 2-decade (1988–2009) record of diatom fluxes in the Mauritanian coastal upwelling: impact of low-frequency forcing and a two-step shift in the species composition. *Biogeosciences*, 18, 1873-1891.

Rosell-Melé, A., Jansen, E. & Weinelt, M. (2002) Appraisal of a molecular approach to infer variations in surface ocean freshwater inputs into the North Atlantic during the last glacial. *Global and Planetary Change*, 34, 143 – 152, doi:10.1016/S0921-8181(02)00111-X.

Royer, T. C., & Grosch, C. E. (2006), Ocean warming and freshening in the northern Gulf of Alaska. *Geophysical Research Letters*, 33, L16605, doi:10.1029/2006GL026767.

Round, F.E., Crawford, R.M. & Mann, D.G. (1990). *The Diatoms. Biology and Morphology of the Genera*. Cambridge University Press, Cambridge.

Sancetta, C. (1981). Oceanographic and ecologic significance of diatoms in surface sediments of the Bering and Okhotsk seas. *Deep-Sea Research*, 28, 789–817.

Sancetta, C., & Calvert, S. E. (1988). The annual cycle of sedimentation in Saanich Inlet, British Columbia: implications for the interpretation of diatom fossil assemblages. *Deep-Sea Research*, 35, 1, 71-90.

Sánchez-Montes, M. L., McClymont, E. L., Lloyd, J. M., Müller, J., Cowan, E. A., & Zorzi, C. (2020). Late Pliocene Cordilleran Ice Sheet development with warm northeast Pacific sea surface temperatures. *Climate of the Past*, 16(1), 299-313, 10.5194/cp-16-299-2020

Schrader, H.-J., & Gersonde, R. (1978). Diatoms and silicoflagellates. In Zachariasse, W. J., Riedel, W. R., Sanfilippo, A., Schmidt, R. R., Brolsma, M. J., Schrader, H., et al. (eds.), *Micropaleontological counting methods and techniques - an exercise on an eight meter section of the Lower Pliocene of Capo Rosello, Sicily*, Utrecht Micropaleontological Bulletin, Utrecht, 17, 129-176.

Schroth, A. W., Crusius, J., Sholkovitz, E. R., & Bostick, B. C. (2009). Iron solubility driven by speciation in dust sources to the ocean. *Nature Geoscience*, 2(5), 337-340.

Schroth, A. W., Crusius, J., Gassó, S., Moy, C. M., Buck, N. J., Resing, J. A., and Campbell, R. W. (2017). Atmospheric deposition of glacial iron in the Gulf of Alaska impacted by the position of the Aleutian Low. *Geophysical Research Letters*, 44(10), 5053-5061, https://doi.org/5010.1002/2017GL073565.

Seguinot, J., Rogozhina, I., Stroeven, A.P., Margold, M., & Kleman, J. (2016). Numerical simulations of the Cordilleran ice sheet through the last glacial cycle. *Cryosphere,* 10, 639–664. doi:10.5194/tc-10-639-2016

Sharon, Belanger, C., Du, J., & Mix, A. (2021). Reconstructing paleo-oxygenation for the last 54,000 years in the Gulf of Alaska using cross-validated benthic foraminiferal and geochemical records. *Palaeoceanography and Paleoclimatology*, 36, e2020PA003986. https://doi.org/10.1029/2020PA003986.

Sikes, E. L., Volkman, J.K., Robertson, L.G. & Pichon, J.-J. (1997). Alkenones and alkenes in surface waters and sediments of the Southern Ocean: Implications for paleotemperature estimation in polar regions. *Geochimica et Cosmochimica Acta*, 61(7), 1495-1505.

Stabeno, P. J., Bond, N. A., Hermann, A. J., Kachel, N. B., Mordy, C. W., & Overland, J. E. (2004). Meteorology and oceanography of the Northern Gulf of Alaska. *Continental Shelf Research*, 24(7), 859-897.

Strom, S. L., Olson, M. B., Macri, E. I., & Calvin, W. M. (2006). Cross-shelf gradients in phytoplankton community structure, nutrient utilization, and growth rate in the coastal Gulf of Alaska. *Marine Ecology Progress Series*, 328, 75-92.

Strom, S. L., Fredrickson, K. A., & Bright, K. J. (2016). Spring phytoplankton in the eastern coastal Gulf of Alaska: Photosynthesis and production during high and low bloom years. *Deep Sea Research Part II: Topical Studies in Oceanography*, 132: 107-121.

Tierney, J. E., & M. P. Tingley. (2018). BAYSPLINE: A New Calibration for the Alkenone Paleothermometer. *Paleoceanography and Paleoclimatology*, 33(3), 281-301. https://doi.org/10.1002/2017PA003201

Walczak, M. H., Mix, A. C., Cowan, E. A., Fallon, S., Fifield, L. K., Alder, J. R., et al. (2020). Phasing of millennial-scale climate variability in the Pacific and Atlantic Oceans. *Science*, 370(6517), 716-720, 10.1126/science.aba7096

Wang, J., Jin, M., Musgrave, D. L., & Ikeda, M. (2004). A hydrological digital elevation model for freshwater discharge into the Gulf of Alaska. *Journal of Geophysical Research: Oceans*, 109(C7), https://doi.org/10.1029/2002JC001430

Wang, K. J., Huang, Y., Majaneva, M., Belt, S.T., Liao, S., Novak, J., et al. (2021). Group 2i Isochrysidales produce characteristic alkenones reflecting sea ice distribution. *Nature Communications*, 12(1), 15, 10.1038/s41467-020-20187-z

Winter, A., Jordan, R. W., & Roth P.H. (1994). Biogeography of living coccolithophores in ocean waters. In: Winter, A., & Siesser, W.G. (Eds.), *Coccolithophores*, Cambridge Univ. Press, New York (1994), pp. 161-178

Wollast, R., & Chou, L. (1998). Distribution and fluxes of calcium carbonate along the continental margin in the Gulf of Biscay. *Aquatic Geochemistry*, 4, 369-393. https://doi.org/10.1023/A:1009640432692

Zindorf, M., Rush, D., Jaeger, J., Mix, A., Penkrot, M. L., Schnetger, B., et al. (2020). Reconstructing oxygen deficiency in the glacial Gulf of Alaska: Combining biomarkers and trace metals as paleo-redox proxies. *Chemical Geology*, 119864, https://doi.org/10.1016/j.chemgeo.2020.119864

Ziveri, P., Baumann, K.-H., Böckel, B., Bollman, J., & Young, J.R. (2004). Biogeography of selected Holocene coccoliths in the Atlantic Ocean. In: Thierstein, H., and Young, J. (eds). *Coccolithophores: from Molecular Processes to Global Impact*. Springer Verlag. pp. 403-428.

Supporting information

1. Mass accumulation rates (MAR)

Superimposed on the orbital-paced forcing of productivity and sea-surface variations of the Site U1419 record for the past 54 kyr, the total MAR is characterized by suborbital-scale variability of diverse amplitudes during MIS 3 and MIS 2 (Figure S1). The abrupt increases in IRD MAR, named Siku Events (SE), lasted between 1,000 and 2,500 years, and are primarily attributed to iceberg discharges from the northern Cordilleran Ice Sheet (CIS, Walczak et al., 2020).

MAR of the measured bulk sedimentary components closely follows the overall pattern of total and ice-rafted debris (IRD) MAR (Figure S1). bSi MAR ranges 0.1-97.1 g cm^{-2} ka^{-1} (average = 12.1±21. 6); $CaCO_3$ MAR ranges 0.3-33.6 g cm^{-2} ka^{-1} (average = 8.4±8.3), and TOC MAR range is 0.01-4.8 g cm^{-2} ka^{-1} (average = 1.2±1.1). Peaks of $CaCO_3$ and TOC MAR better match the temporal pattern of total MAR than bSi MAR. Carbonate and TOC MARs peak during Siku Events (SE) 1-4. The highest MAR for carbonate occurs during SE 1 (33.6 g/cm^2/ka) and ~34 ka (33. 5 g/cm^2/ka). TOC peaks during SE 1 (4.8 g/cm^2/ka) and SE4 (4.8 g/cm^2/ka). Exceptions to this pattern are $CaCO_3$ MAR peaks at c. 39 ka (Heinrich stadial 4, 18.1 g/cm^2/ka) and at c. 24 ka (Heinrich stadial 2, 23.0 g/cm^2/ka, respectively, Figure S1). Additionally, peaks in both carbon species MAR are observed from 20-22 ka and ~34 ka. MAR TOC has an additional maximum between ~43-46 ka (2.3-2.5 g/cm^2/ka). The highest bSI MAR (81-97 g/cm^2/ka) occurs between 44-45 kyr. Two others high bSi MARs are during SE4 and SE1. The increases in carbonate and TOC MAR during the SEs may reflect enhanced preservation due to increased burial rates or the addition of terrestrially derived components. The different temporal patterns between MAR and concentration of bulk sediment components suggests that these biogenic maxima were impacted by enhanced burial efficiency caused by high sediment accumulation and/or the meltwater-related discharges from the CIS along the northern Alaska margin.

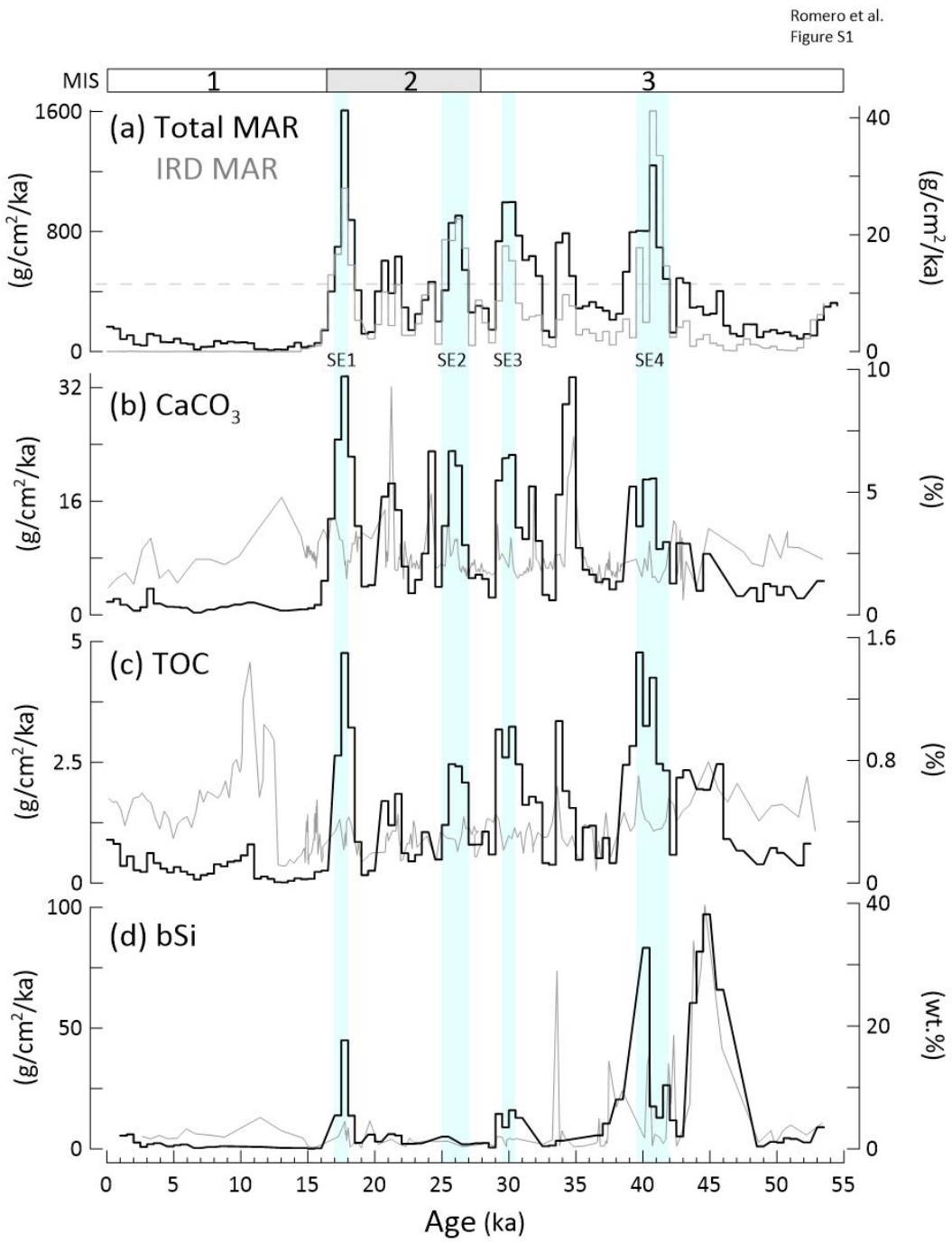

Figure S1. Mass accumulation rate (black bars) and concentration (grey line) of bulk biogenic components at IODP Site U1419 for the past 54 ka. (a) Total MAR (black line) and ice-rafted debris (IRD) MAR (grey line) (g/cm^2/ka) from Walczak et al. (2020); (b) $CaCO_3$ (; g/cm^2/ka and %); (c) total organic carbon (TOC; g/cm^2/ka and %) and (d) bSi (g/cm^2/ka and wt.%). After Walczak et al. (2020), sedimentation and mass accumulation rates are evaluated over constant timestep bins of 500 years to avoid interpretive artifacts associated with varying sample resolution. Light blue bars denote Siku Events (SE) 1-4 where IRD MAR exceeds 12 g cm^2 ka^{-1} ((a), dashed line). All data are binned at 500 years (Walczak et al., 2020). MIS: Marine Isotope Stage.

The MAR of diatoms ranges 0-2.0*10^9 valves cm^{-2} ka^{-1} (average = 1.5*10^8±4.4*10^8, Figure S2). Highest diatom MAR was reached between 44.6 and 39 ka. A second highest maximum

occurred around 33.6 ka. Total C37 alkenone MAR show large millennial-scale variability, recording peaks in the early Holocene (10 ka) and during SE 1-3 (Figure S2). No alkenone MAR data is available for SE4. There are also increases in alkenone MAR between SE 1-3, and the largest peak in alkenone-MAR is recorded before SE 4 (at 48-43 ka).

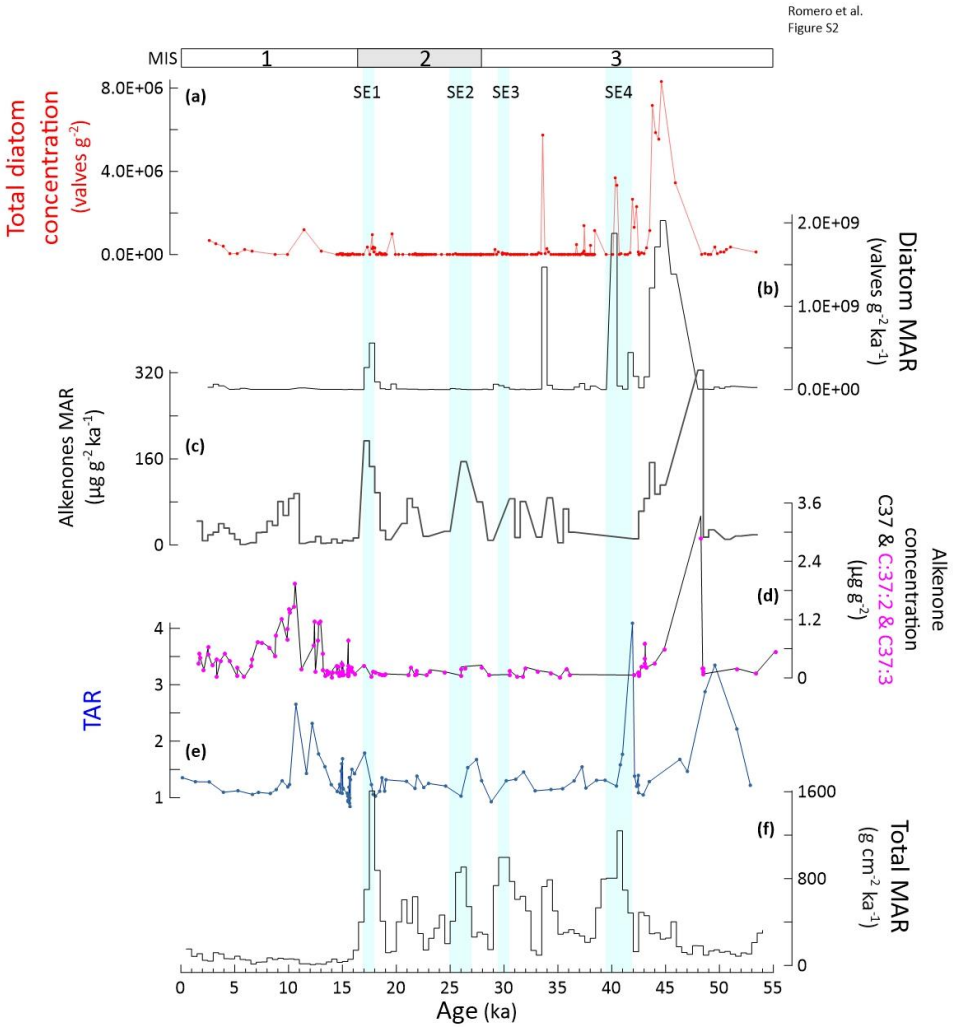

Figure S2. Mass accumulation rate (MAR) and concentration of proxies at IODP Site U1419 for the past 54 ka. (a) total diatom concentration (valves g^{-2}, red line); (b) diatom MAR (valves g^{-2} ka^{-1}); (c) total C37 alkenone MAR (µg cm^{-2} ka^{-1}); (d), total C37 (black line) and C37:3+C32:2 concentration (magenta dots) (µg g^{-2}); (e) Terrestrial aquatic ratio (TAR), and (f) Total MAR (black line) (g/cm^2/ka; Walczak et al., 2020). After Walczak et al. (2020), sedimentation and mass accumulation rates are evaluated over constant timestep bins of 500 years to avoid interpretive artifacts associated with varying sample resolution. Light blue bars denote Siku Events (SE) 1-4 where IRD MAR exceeds 12 g cm^2 ka^{-1} ((a), dashed line). All data are binned at 500 years (Walczak et al., 2020). MIS: Marine Isotope Stage.

2. Alkenone calibrations

Several different alkenone calibrations are available for high-latitude samples, which give different absolute SST reconstructions and interpretations. The original core-top calibration

(Müller et al., 1998) aligns very closely to a culture of *Emiliania huxleyi* (Prahl et al., 1988), and both are extensively used to reconstruct mean annual SST through time. However, analysis of surface sediments in the eastern North Pacific showed an under-estimation of observed SSTs, leading the authors to propose that a Southern Ocean calibration by Sikes et al. (1997) was more appropriate, and that summer SSTs were recorded (Méheust et al., 2013). A summer signal in $U^{K'}_{37}$ was also suggested by elevated alkenone-SSTs in surface sediments from GoA (Prahl et al., 2010), close to Site U1419. A recent Bayesian calibration for globally-distributed core-top data (BAYSPLINE, Tierney & Tingley, 2018), also identifies a summer signal in $U^{K'}_{37}$ for the North Pacific. BAYSPLINE gives median reconstructed SSTs at Site U1419 which are -0.45 ± 0.07°C of the values generated using Müller et al. (1998), but with a seasonal not annual signal. For consistency with our previous SST reconstructions in the GoA (Müller et al., 2018; Sanchez-Montes et al., 2020), and given the close similarity between BAYSPLINE and the Müller et al. (1998) calibration (Figure S3), we apply the Müller et al. (1998) calibration here, acknowledging that this likely gives a summer SST reconstruction.

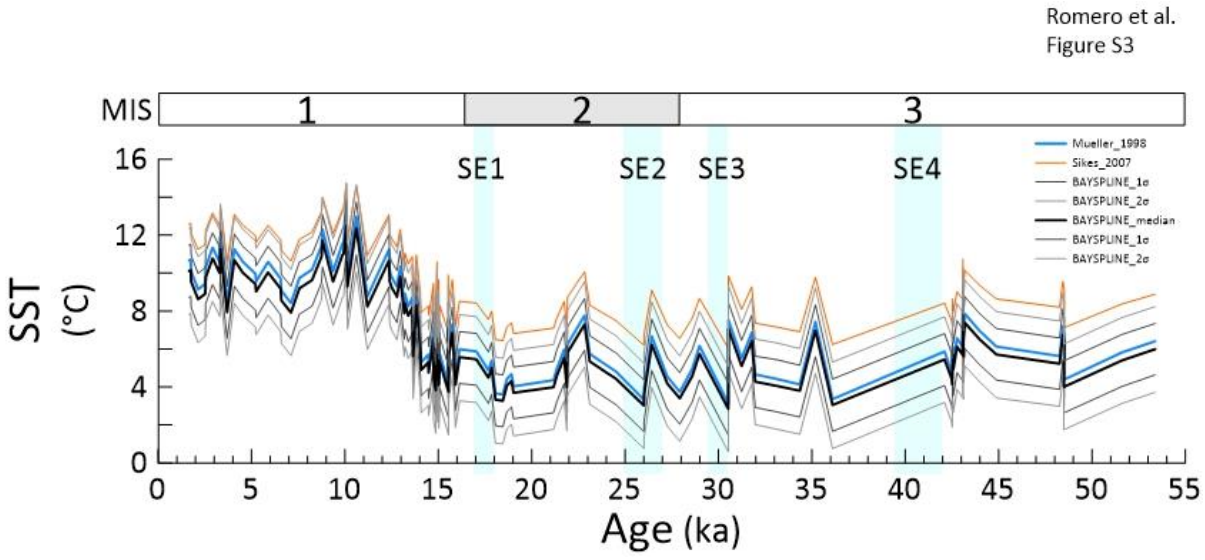

Figure S3. A comparison of the impact of different $U^{K'}_{37}$ calibrations on the absolute SSTs reconstructed at IODP site U1419. We apply the linear Mueller et al. (1998) in the main manuscript and show here the close similarity to the more recent Bayesian calibration (BAYSPLINE, Tierney & Tingley, 2018) which is calibrated against summer SSTs. A Southern Ocean calibration (Sikes et al. 1997) is also applied, as recommended by Méheust et al. (2013), which is offset from the two other calibrations. The overall trends and patterns in the data are unchanged regardless of the calibration used.

3. Composition of the diatom groups at the IODP Site U1419 for the past 54 ka. The groups and the species within each group are ordered alphabetically.

Group	Species	Main paleocological conditions	Main reference/s
Low productivity, coastal cold waters	*Coscinodiscus argus* *Coscinodiscus oculus-iridis* *Cyclotella litoralis* *Thalassiosira gravida* *Thalassiosira grunowii* *Thalassiosira trifulta*	Low nutrient availability in surface coastal waters	Crosta et al. (2012) Hasle & Syvertsen (1996) Romero & Armand (2010) Sancetta (1981)
High productivity, coastal waters	Resting spores of *Chaetoceros* spp. *Thalassionema nitzschioides* var. *nitzschioides*	High nutrient availability in the uppermost water column	Nave et al. (2001) Romero & Armand (2010)
Neritic waters	*Actinocyclus curvatulus* *Actinocyclus oculatus* *Actinocyclus octonarius* *Actinoptychus senarius* *Adoneis pacifica* *Amphora* spp. *Cocconeis* spp. *Delphineis kippae* *Grammatophora* spp. *Nitzschia palea* *Odontella aurita* *Opephora* spp. *Paralia sulcata*	Grow in shore and shallow waters, attached to a substratum. Their occurrence in hemipelagic sediments represents a transport signal from shallow into deeper waters.	Round et al. (1990) Sancetta (1981)
Pelagic cold waters	*Fragilariopsis fossilis* *Fragilariopsis oceanica* *Rhizosolenia hebetata* f. *hiemalis* *Rhizosolenia hebetata* f. *semispina* *Stellarima* spp. *Thalassiosira anguste-lineata* *Thalassiosira leptopus* *Thalassiosira minutissima* *Thalassiosira nordenskioeldii* *Thalassiosira robusta* *Thalassiosira sancettae*	Represent the influence of open-ocean, cold water masses	Hasle & Syvertsen (1996) Romero & Armand (2010) Sancetta (1981)
Pelagic temperate waters	*Azpeitia neocrenulata* *Azpeitia tabularis* *Nitzschia challengerii* *Roperia tesselata* *Shionodiscus oestrupii* var. *oestrupii* *Shionodiscus oestrupii* var. *venrickae* *Stephanopyxis* spp. *Thalassiosira eccentrica* *Thalassiosira ferelineata* *Thalassiosira nannolineata* *Thalassiosira robusta*	Mainly thriving in the low to mid latitude (40°N – 40°S) open ocean. They represent the possible northward transport of warm to temperate waters	Crosta et al. (2012) Nave et al. (2001) Romero et al. (2005) Romero et al. (2021)
Sea-ice associated	*Bacterosira* spp. *Fragilariopsis cylindrus* *Porosira glacialis* *Thalassiosira antarctica* (vegetative cells and spores)	They occur within, on or under sea ice or in waters closely surrounding sea ice	Barron et al. (2009) Hasle & Syvertsen (1996) Sancetta (1981)

Supporting references

Barron, J. A., Bukry, D., Dean, W.E., Addison, J. A., & Finney, B. (2009). Paleoceanography of the Gulf of Alaska during the past 15,000 years: Results from diatoms, silicoflagellates, and geochemistry. *Marine Micropaleontology*, 72(3), 176-195.

Crosta, X., Romero, O. E., Ther, O. & Schneider, R. R. (2012). Climatically-controlled siliceous productivity in the eastern Gulf of Guinea during the last 40 000 yr. *Climate of the Past*, 8(2), 415-431. 10.5194/cp-8-415-2012

Hasle, G. A. & Syvertsen, E. E. (1996), Marine diatoms, IN: Identifying marine diatoms and dinoflagellates, edited by: Thomas, C., Academic Press, Inc. San Diego, CA, 1–385, 1996.

Méheust, M., Fahl, K. & Stein, R. (2013). Variability in modern sea surface temperature, sea ice and terrigenous input in the sub-polar North Pacific and Bering Sea: Reconstruction from biomarker data. *Organic Geochemistry*, 57, 54-64.

Müller, P.J., Kirst, G., Ruhland, G., von Storch, I., & Rosell-Melé, A. (1998). Calibration of the alkenone palaeotemperature index UK-37 based on core-tops from the eastern South Atlantic and the global ocean (60°N–60°S). *Geochimica et Cosmochimica Acta*, 62, 1757–1772.

Müller, J., Romero, O.E., Cowan, E.A. McClymont, E.L., Forwick, M.et al. (2018). Cordilleran ice-sheet growth fueled primary productivity in the Gulf of Alaska, northeast Pacific Ocean. *Geology*, 46, 307-310.

Nave, S., Freitas, P., & Abrantes, F. (2001). Coastal upwelling in the Canary Island region: spatial variability reflected by the surface sediment diatom record. *Marine Micropaleontology,* **42**), 1-23. https://doi.org/10.1016/S0377-8398(1001)00008-00001.

Prahl F. G., Muelhausen L. A., & Zahnle D. L. (1988) Further evaluation of long-chain alkenones as indicators of paleoceanography conditions. *Geochimica et Cosmochimica Acta*, 52, 2303–2310.

Prahl, F. G., Rontani, J. F., Zabeti, N., Walinsky, S. E., & Sparrow, M. A. (2010). Systematic pattern in U37K' – Temperature residuals for surface sediments from high latitude and other oceanographic settings. *Geochimica et Cosmochimica Acta*, 74(1), 131-143.

Romero, O. E., Armand, L. K., Crosta, X., & Pichon, J. J. (2005). The biogeography of major diatom taxa in Southern Ocean surface sediments: 3. Tropical/Subtropical species. *Palaeogeography, Palaeoclimatology, Palaeoecology*, 223, 49-65.

Romero, O. E., & Armand, L. K. (2010). Marine diatoms as indicators of modern changes in oceanographic conditions. In: Smol, J. P., Stoermer, E. F. (Eds.), *The Diatoms, Applications for the Environmental and Earth Sciences* (Second Edition (pp. 373-400). Cambridge University Press, Cambridge.

Romero, O. E., Ramondenc, S., & Fischer, G. (2021). A 2-decade (1988–2009) record of diatom fluxes in the Mauritanian coastal upwelling: impact of low-frequency forcing and a two-step shift in the species composition. *Biogeosciences*, 18, 1873-1891.

Round, F.E., Crawford, R.M. & Mann, D.G. (1990). *The Diatoms. Biology and Morphology of the Genera*. Cambridge University Press, Cambridge.

Sancetta, C. (1981). Oceanographic and ecologic significance of diatoms in surface sediments of the Bering and Okhotsk seas. *Deep-Sea Research*, 28, 789–817.

Sánchez-Montes, M. L., McClymont, E. L., Lloyd, J. M., Müller, J., Cowan, E. A., & Zorzi, C. (2020). Late Pliocene Cordilleran Ice Sheet development with warm northeast Pacific sea surface temperatures. *Climate of the Past*, 16(1), 299-313, 10.5194/cp-16-299-2020

Sikes, E. L., Volkman, J.K., Robertson, L.G. & Pichon, J.-J. (1997). Alkenones and alkenes in surface waters and sediments of the Southern Ocean: Implications for paleotemperature estimation in polar regions. *Geochimica et Cosmochimica Acta*, 61(7), 1495-1505.

Tierney, J. E., & M. P. Tingley. (2018). BAYSPLINE: A New Calibration for the Alkenone Paleothermometer. *Paleoceanography and Paleoclimatology*, 33(3), 281-301. https://doi.org/10.1002/2017PA003201

Walczak, M. H., Mix, A. C., Cowan, E. A., Fallon, S., Fifield, L. K., Alder, J. R., et al. (2020). Phasing of millennial-scale climate variability in the Pacific and Atlantic Oceans. *Science*, 370(6517), 716-720, 10.1126/science.aba7096